
Scaling Turbulence in the Planetary Boundary Layer

G.A. McBean

Atmospheric Environment Service, Downsview, Ontario

[Manuscript received 14 January 1976; in revised form 10 August 1976]

ABSTRACT

Two different approaches to scaling turbulence in the planetary boundary layer over Lake Ontario are investigated. The height up to the inversion was found to be the appropriate scaling height while u_* for near-neutral

and w_* for unstable conditions were the appropriate scaling velocities. The results were in general agreement with the numerical models of Deardorff (1972) and Wyngaard, Cote, and Rao (1974).

1 Introduction

One characteristic that distinguishes the planetary boundary layer (pbl) from the atmosphere above it is the almost continuous distribution in space and time of turbulent motion. The turbulence is responsible for the transfers of momentum, heat, and matter, for the bouncing of an aircraft on ascent or descent, and for the buffeting of tall structures. Although a comprehensive theory of the pbl is lacking, much progress has been made in numerically modelling the pbl (e.g. Deardorff, 1973). There is still a need, however, for experimental data against which these models can be compared. The data are also valuable for the development of empirical relationships, which are very useful for practical applications.

In this paper an analysis of data collected during the International Field Year on the Great Lakes (IFYGL) is presented. The turbulence data were obtained by the National Aeronautical Establishment T-33 jet aircraft, specially instrumented for turbulence measurements, and have been described by McBean and MacPherson (1976) and McBean and Paterson (1975). The buoy and radiosonde data were collected as part of the IFYGL basic data set and are available from the IFYGL data banks. It is proposed to consider the scaling of the turbulence as a function of height and stability. First, two possible scaling schemes for pbl turbulence will be described. Then a comparison of the two schemes will be presented and, finally, some empirical formulas will be given in the hope that they will be useful in some applications. The results will be compared, as well, with the numerical model results of Wyngaard, Cote, and Rao (1974; hereafter cited as WCR) and Deardorff (1972; hereafter cited as D72).

2 Turbulence scaling parameters

Although there are many possible ways of scaling turbulence, only the two most widely used will be considered. To represent the turbulence the standard deviations of the fluctuations of the three velocity components and virtual temperature and the fluxes of momentum and virtual heat will be used. The scaling will then be in non-dimensional form, i.e.

$$\sigma_x/P_x = G_x(z/P_z, S)$$

and

$$F_x/D_x = C_x(z/P_z, S)$$

where σ_x is the standard deviation of the fluctuations of x ,

F_x is the flux of x ,

D_x, P_x, P_z are the scaling parameters,

z is the height

S is the stability

and G_x, C_x are unknown functions which will be different for each x .

For each scaling scheme we need a scaling velocity, a scaling temperature, a scaling height, and a non-dimensional number to represent stability. Because there is some latitude in choosing these scales it is necessary to consider the physical basis for the scaling. In analogy with surface-layer scaling (see, e.g. Wyngaard, 1973) we can use for scaling velocity and temperature:

$$u_* = \{\tau/\rho\}^{1/2} \text{ where } \tau \text{ is the surface stress,}$$

$$T_* = -Q/u_* \text{ where } Q \text{ is the virtual temperature flux;}$$

and for stability, a height divided by the Monin-Obukhov length, $L = u_*^2 T / kg T_*$ where k is von Kármán's constant ($= 0.4$). For the neutral barotropic pbl the relevant scaling height is cu_*/f (Tennekes, 1973), where f is the magnitude of the Coriolis parameter and c is an undetermined constant with a value between 0.2 and 0.5.

For convective conditions an alternate surface layer scaling is:

$$u_f = (zgQ/T)^{1/3}$$

$$T_f = (Q^2 T / gz)^{1/3}$$

Deardorff (1973) has found for unstable conditions that u_*/f was not a relevant height and that h , the depth of the unstable layer under the inversion, was more pertinent. Then, pbl scaling velocities and temperatures are

$$w_* = (hgQ/T)^{1/3}$$

and $\theta_* = (Q^2 T / gh)^{1/3}$.

We thus have two sets of scaling parameters as summarized in Table 1. Note that all the parameters are independent of height since they are defined in terms of the surface stress and heat flux and the height of the inversion. T is a representative temperature of the layer. It should also be noted that these simple scaling schemes may be an oversimplification. For second-order effects more complicated schemes will likely be needed.

TABLE 1. Two possible sets of scaling and stability parameters

	(a)	(b)
velocity	u_*	w_*
temperature	T_*	θ_*
height	cu_*/f	h
stability	cu_*/fL	h/L

The bulk transfer equations

$$u_*^2 = C_D \bar{u}_{10}^2$$

$$Q = C_D \bar{u}_{10} ((T_w - T_a) + 0.61T(q_* - q_a))$$

$$C_D = (0.58 + 0.068\bar{u}_{10}) \times 10^{-3} \quad (\bar{u} \text{ in m s}^{-1}; \text{ Smith, 1973})$$

were used to compute the surface stress and vertical heat flux, as in McBean and Paterson (1975). The height of the inversion was determined by examining the radiosonde data around the lake and deducing what the profile over the lake would look like. There is a considerable amount of subjectivity in determining h and the errors could be significant.

3 Results

The observations were made on 8, 9, 12 and 15 October 1972 and only flight legs over the lake are considered. Most of the flights (43) were flown 150 m above the lake with some at 30 m (5), 60 m (8), and 300 m (7) for a total of 63 flights. The flights were generally 45 km (6 min at 125 m s^{-1}) in length and were flown at various angles to the mean wind. On all days there was scattered-to-broken cumulus and stratocumulus clouds. Cloud bases were generally 800–1500 m above the surface and often within the boundary layer. All flights were flown well below cloud bases. In order to separate the effects of stability from those of height the data were divided into stability groups dependent on either cu_*/fL or h/L (Table 2). The number of groups for h/L was smaller because the stability variations were expected to be smaller.

In Fig. 1 the heights h and $0.5 u_*/f$ are compared. For Group A the points scatter but most fall near the line $h \sim 0.3 u_*/f$. The points in the lower right sector were for cases of significant baroclinicity. For Group C the points are near $h \sim 0.5 u_*/f$ with the points for Group B being intermediate. The D72

TABLE 2. Stability classifications

$0.5u_*/fL$			h/L		
Group	Range	No. of Obs	Group	Range	No. of Obs
I	0:–10	17	A	0:–12	33
II	–10:–20	16	B	–12:–34	11
III	–20:–40	11	C	–34:–65	19
IV	–40:–50	12			
V	–50:–70	7			

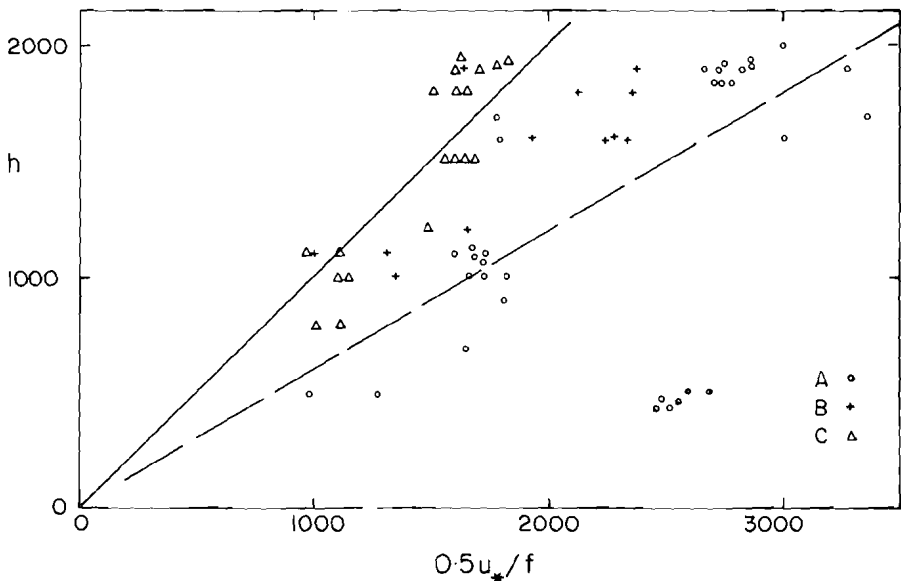


Fig. 1 The relationship between the height up to the inversion, h , and the dynamic height, $0.5 u_* / f$, for each of the three stability groups A, B, C. The solid line is $h = 0.5 u_* / f$ and the dashed line is $h = 0.3 u_* / f$.

modelling studies indicate that h is not related to u_* / f . Both D72 and WCR found the height of the momentum boundary layer for the neutral case to be $0.3 u_* / f$. Since h is the height of the thermal boundary layer and is poorly defined for near neutral conditions, it may be only coincidental that $h \sim 0.3 u_* / f$ was found here for Group A.

Vertical velocity fluctuations

In order to objectively determine which scaling gave the best fit to the data, the following procedure was used. Each variable was non-dimensionalized with either u_* , w_* , etc. and plotted against z/h or zf/cu_* for each stability group. Then polynomials (up to order 3) were fitted by the method of least squares and the scaling scheme that most reduced the variance was accepted as best. For Group I the best approach was σ_w / u_* vs z/h . For each of Groups II to V, σ_w / w_* vs z/h was as good or better than any other scheme. This result was expected and is in agreement with D72. An advantage of the σ_w / w_* vs z/h scaling is that the stability dependence of the relationship was negligibly small. h was the most appropriate scaling height in all cases so it seems more appropriate to look at stability groupings A, B, C. It was found that w_* and h scaling was most appropriate for all three stability groupings. The reduction in variance by grouping on basis of h/L was generally better than the groupings based on cu_* / fL .

It is somewhat surprising that w_* and h proved to be the better scaling system for Group A. It was expected that u_* and u_* / f scaling would be more appro-

priate for the near neutral cases. Clarke and Hess (1973) found for the Wangara mean wind and temperature profiles that u_*/f scaling was better than h for all cases. To investigate the effects near neutral, those cases with $-h/L < 3$ were considered separately. The scaling combination (w_*, h) was again the best. The ratios of the standard deviation from the best-fit, third-order polynomial to the standard deviation from the mean were: (w_*, h) , 0.41; $(u_*, u_*/f)$, 0.64; (u_*, h) , 0.79; and $(w_*, u_*/f)$, 0.84. It should be noted that ten of the twelve cases in this subgroup had h/L values between 2 and 3 and for all cases $z < L$. Surface layer measurements (McBean, 1971; Wyngaard, 1973) have shown the onset of local free convection for $z \sim |0.4L|$. Seven of the twelve cases in this subgroup have $z > |0.4L|$ and hence local free convection is possible. Because of the small number of cases, it is not possible to further subdivide the data. The energy input by buoyancy affects most directly the vertical velocity and temperature fluctuations. This may be the reason why these data scale better with (w_*, h) while Clarke and Hess found $(u_*, u_*/f)$ preferable.

In Fig. 2 the variations of σ_w/u_* (Group A) and σ_w/w_* (all Groups) with z/h are shown. There is no difference between the Groups for h/L scaling. WCR found no variation of σ_w/w_* with h/L for $-50 < h/L < -10$ but their results for σ_w/w_* and those of D72 are larger than those presented here.

Horizontal velocity fluctuations

The velocity fluctuations in the longitudinal, u , and lateral, v , directions did not scale as well as the vertical velocity fluctuations. This characteristic has been observed in most other studies and can be attributed to the effects of large scale spatial or temporal inhomogeneities that are not accounted for in the scaling schemes. For the longitudinal component (u_*, h) was best for Groups I and A although $(u_*, u_*/f)$ also gave good results. For the more unstable groups (w_*, h) was the preferable scheme. For the lateral component, the results were not as consistent and the scaling frequently did not reduce the variance to the level of 1% significance (Brooks and Carruthers, 1953, p. 303). For Group A (w_*, h) was best and for Group B (w_*, h) and (u_*, h) equal. For Group C no scheme was statistically significant.

In Figs 3 and 4 the scaled results for σ_u and σ_v are given. For Group A the results, scaled by (u_*, h) , are quite scattered with an indication of a decrease in σ_u and σ_v with z/h increasing. The model computations of D72 and WCR bracket most of the data points, except for z/h near 0.35 where there are several measured values of both σ_u and σ_v that seem too large. There are also two cases for $z/h \sim 0.09$ with large values; these were for adjacent flight legs and it appears that the surface wind estimate is anomalously low.

For the unstable group (Groups B and C together) there is the same amount of scatter with a slight increase of σ_u/w_* and σ_v/w_* with z/h . The results are in approximate agreement in magnitude with D72 and WCR. However, since the D72 model predicts a decrease with z/h and the WCR model predicts an increase, a detailed comparison is not worthwhile.

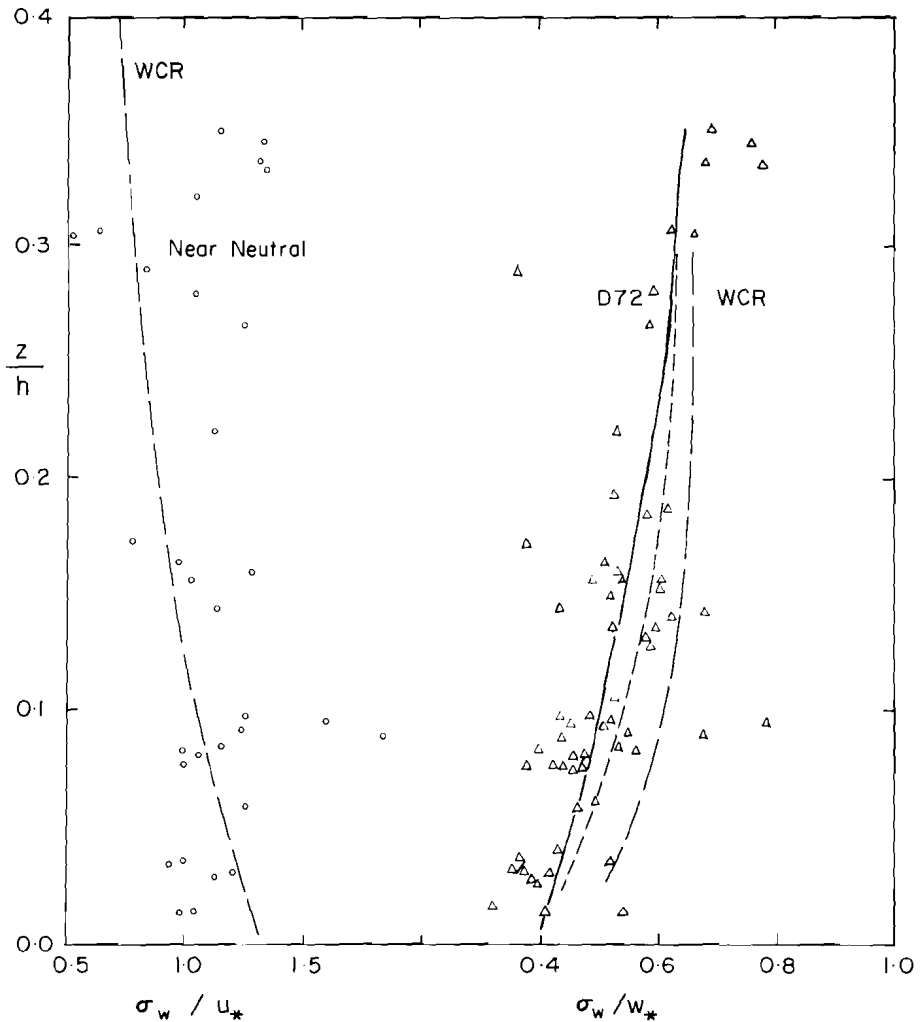


Fig. 2 Non-dimensional standard deviations of vertical velocity fluctuations against the non-dimensional height, z/h . On the left are the near-neutral data (Group A), non-dimensionalized with u_* ; on the right are the data non-dimensionalized with w_* . The WCR curve at the left is for $h/L = 0$, at the right $h/L = -50$ and the D72 curve is for $h/L = -45$. The solid curve on the right is $\sigma_w/w_* = 0.40 + 1.1 z/h - 1.1 (z/h)^2$.

Virtual temperature fluctuations

The virtual temperature fluctuations, θ_v , were not measured directly but can be related to temperature, θ , and humidity, q' , fluctuations by,

$$\theta_v = \theta(1 + 0.61\bar{q}) + 0.61q'T - 0.61\bar{q}\theta$$

The variance is then

$$\begin{aligned} \overline{\theta_v^2} = & \overline{\theta^2} (1 + 0.61\bar{q})^2 + (0.61T)^2 \overline{q'^2} \\ & + 2(1 + 0.61\bar{q}) 0.61T \overline{\theta q'} + 0.37 (\overline{q'\theta})^2 \end{aligned}$$

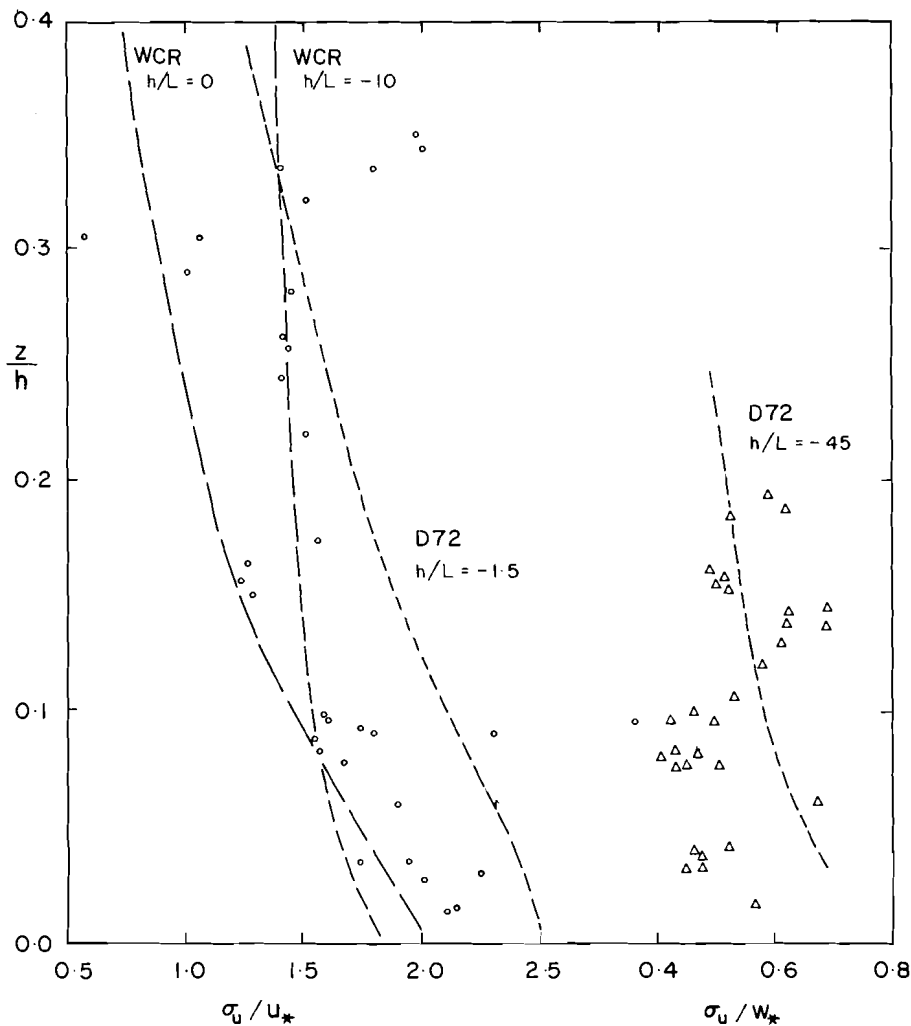


Fig. 3 Non-dimensional standard deviations of longitudinal velocity fluctuations against the non-dimensional height, z/h . On the left are the near-neutral data (Group A), non-dimensionalized with u_* ; on the right are the unstable data (Groups B and C), non-dimensionalized with w_* . The WCR and D72 curves are for the stabilities indicated.

The fourth term can be shown to be negligible in comparison to the others. The other three terms are of the same order. However, the correlation $\overline{\theta \bar{q}}$ was not computed in the data processing. Therefore, the results to be presented are for

$$\sigma_{\theta_v} = \sigma_{\theta}(1 + 0.61\bar{q}) + 0.61T\sigma_q$$

and hence may be about 30% underestimated. The variations with height and stability, however, should not be greatly affected.

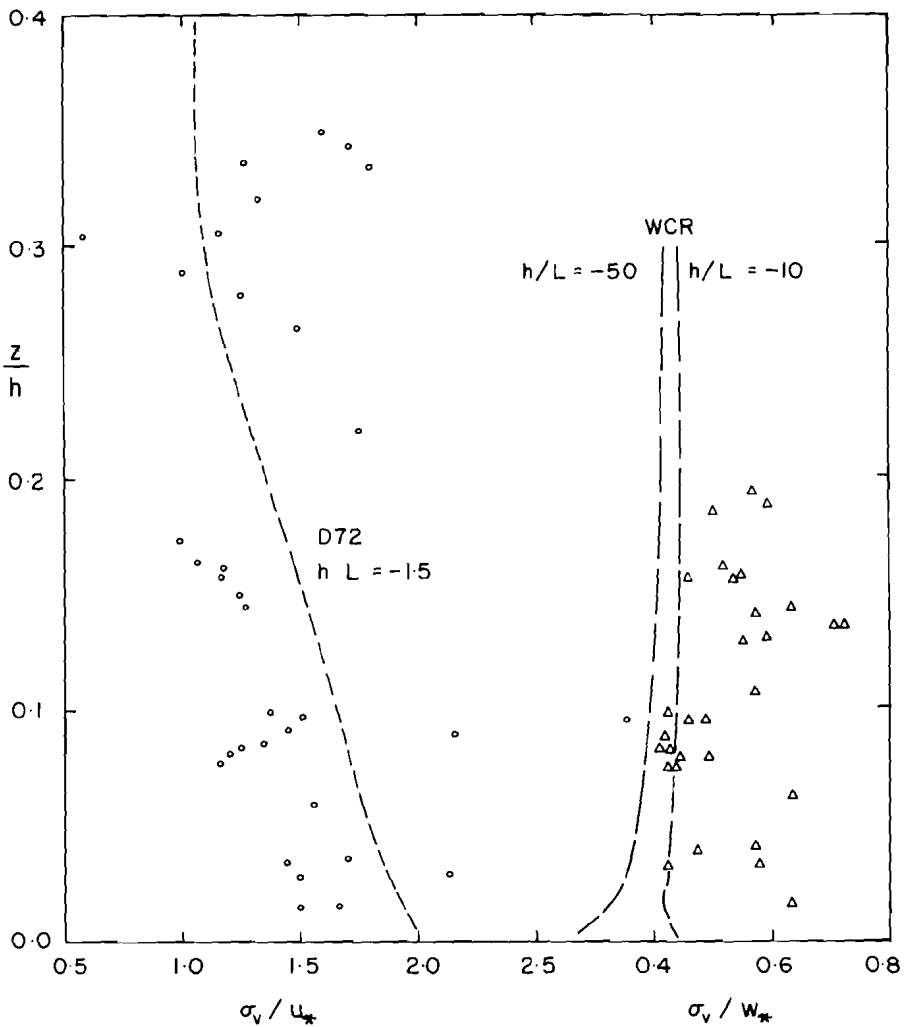


Fig. 4 Non-dimensional standard deviations of lateral velocity fluctuations against the non-dimensional height, z/h . (See Fig. 3).

For the near neutral group the data were quite scattered because of relatively low magnitudes for σ_{θ_v} , θ_* , and T_* . For the unstable groups, h and θ_* are the best scaling parameters. The results (Fig. 5) show an increase of $\sigma_{\theta_v}/\theta_*$ with increasing z/h and are in reasonable agreement with D72 and WCR.

Momentum flux

The momentum flux is one of the most difficult variables to measure experimentally. The results here were no different. The data showed a large amount of scatter regardless of the scaling scheme. The scatter may be due to baroclinic effects and entrainment of air from above $z = h$, as discussed by Deardorff

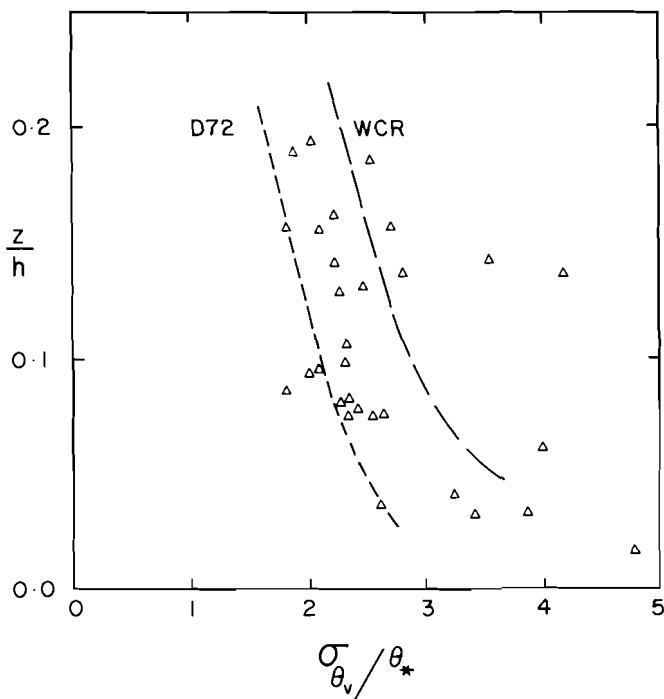


Fig. 5 Non-dimensional standard deviations of potential temperature fluctuations against the non-dimensional height, z/h , for the unstable Groups B and C. The WCR and D72 curves are for $h/L = -50$ and -45 , respectively.

(1973). In Fig. 6 is \overline{uw}/u_*^2 vs z/h for Group A. For comparison, the model results of WCR for $h/L = 0, -2$ and -10 are shown. All that can be said is that the results do not disagree significantly. For the unstable groups the data are very scattered and not shown. The \overline{vw}/u_*^2 term was generally very small for small z/h and increased with z/h . The amount of scatter was again very large.

Virtual heat flux

The virtual heat flux can be computed as

$$\overline{w\theta_v} = \overline{w\theta} (1 + 0.61\overline{q}) + 0.61T \overline{wq'}$$

because the third order terms can be shown to be negligible. The virtual heat fluxes were very small for the near-neutral group and the ratio $\overline{w\theta_v}/Q$ decreased from near unity at $z/h = 0$ to 0 about $z/h \sim 0.3$ as shown in Fig. 7a. The shape is similar to that for momentum flux and indicates that the momentum and heat flux boundary layers are similar in depth ($z \sim 0.3 h$). For Groups B and C (Fig. 7b), the data were also quite scattered. The best-fit straight line for Group C ($\overline{w\theta_v}/Q = 0.76 - 0.99 z/h$, $\Gamma_{xy} = 0.32$) is shown. A second order

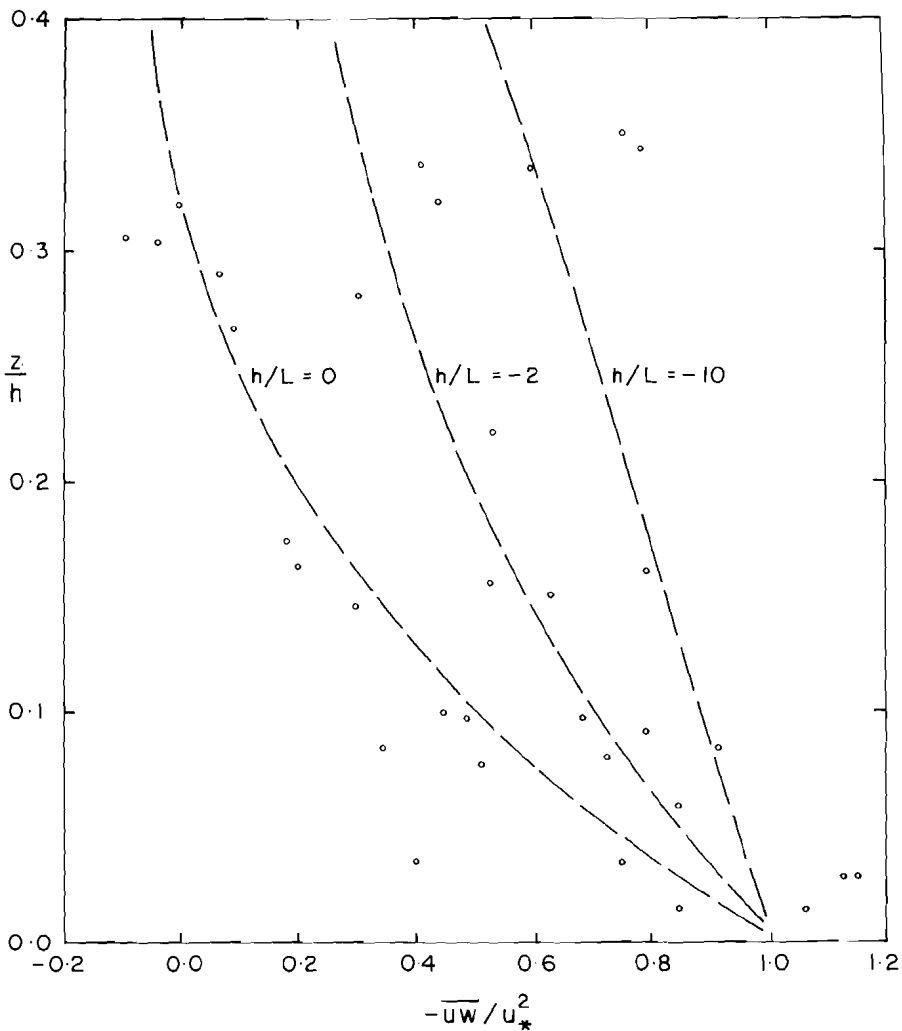


Fig. 6 Non-dimensional momentum flux or stress against the non-dimensional height z/h for the near-neutral Group A. The three dashed curves are all from WCR for the stabilities indicated.

polynomial fit did not significantly reduce the variance. When the analysis was done on Groups I to V it was found that linear fits had relatively high correlations for Groups I, II, and V. Extrapolations to $\overline{w\theta_v}/Q = 0$ gave values $z/h = 0.14$ (Group I), 0.37 (Group II) and 0.68 (Group V). Thus, it seems that the heat flux boundary layer becomes deeper and approximates the height up to the inversion layer for unstable conditions. Lenschow (1970) found the heat flux equal to zero near $z/h = 0.8$ from measurements in an unstable boundary layer.

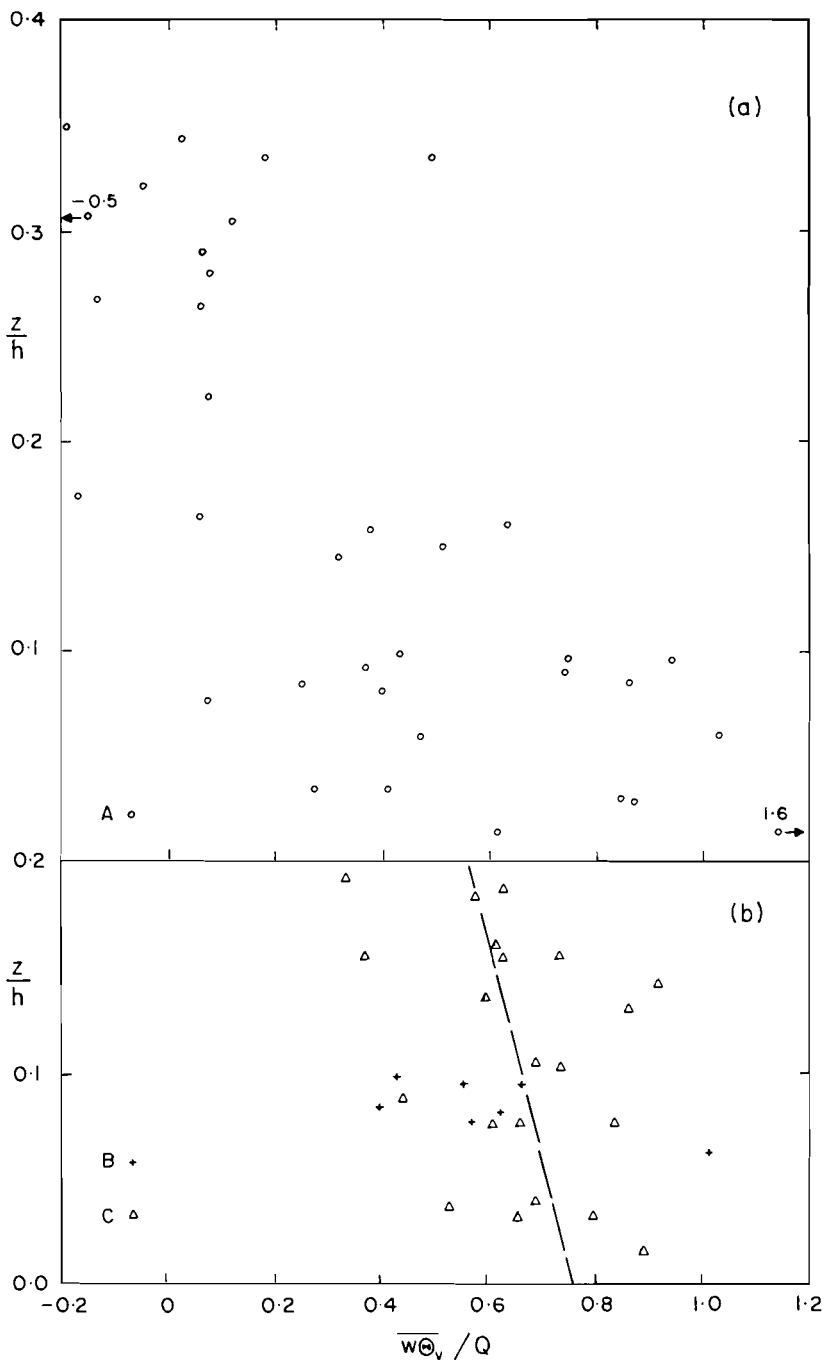


Fig. 7 Non-dimensional heat flux against the non-dimensional height, z/h for the near-neutral Group A (above) and unstable Groups B(+) and C(Δ), (below).

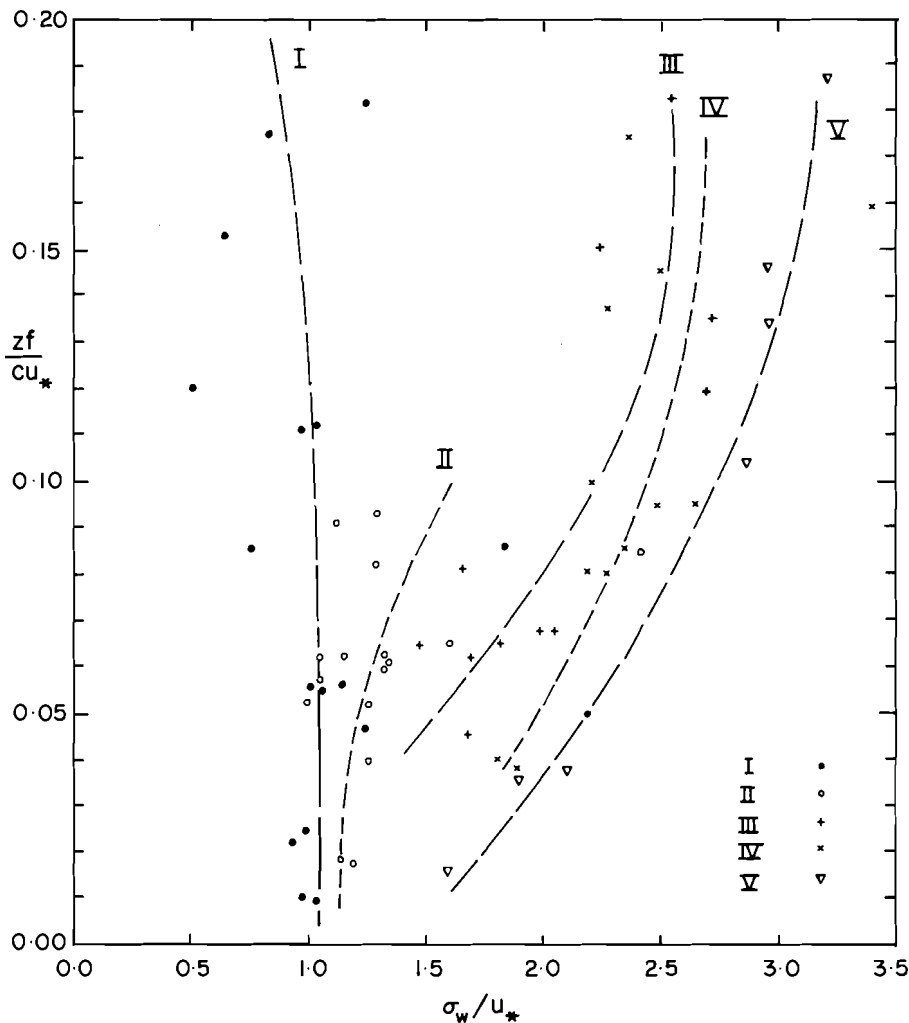


Fig. 8 Non-dimensional standard deviation of vertical velocity fluctuations against non-dimensional height, zf/cu_* ($c = 0.4$), for each stability group (I to V). The curves indicated are best fit polynomials (to order 3) to each group.

4 Practical considerations

As shown in the previous section, the best scaling parameters were h , w_* and θ_* which requires knowledge of the height to the inversion as well as the surface heat flux. An advantage of the cu_*/f , u_* and T_* scaling is that they can be specified with knowledge of the surface values only. There is no need to know the height up to the inversion. For practical reasons then the cu_*/f scaling may be more useful, particularly for those concerned with the intensity of the turbulence as a function of height.

In Fig. 8 the variations of σ_w/u_* with height and stability are demonstrated.

As shown, there is an increase of σ_w/u_* with stability at a given non-dimensional height. For near-neutral stabilities σ_w/u_* is about constant or slowly decreasing with z/cu_* while for unstable stratifications there is a marked increase with z/cu_* . For practical purposes one could use:

$\sigma_w/u_* \sim 1.1 - 1.6 z/cu_*$ for near-neutral conditions, which reduces to $\sigma_w/u_* \sim 1.0$ for neutral stratifications, and $\sigma_w/u_* \sim 1.1 + 42 z/cu_* - 300 (z/cu_*)^2$ for unstable stratifications (the curve for Group IV). These expressions would be valid for $z < 0.1 u_*/f \sim 10^3 u_*$ (mid-latitudes). For over water this would be $z < 30 \bar{u}_{10}$. Over land it will be more difficult to determine u_* from the mean wind and it is possible that the results may depend on the surface Rossby number G/fz_0 where G is the geostrophic wind speed and z_0 the roughness length.

For σ_u/u_* and σ_v/u_* the results were similar to those for σ_w/u_* but with a larger amount of scatter. For Groups I and II the curves were similar with both parameters decreasing slightly with height. The best straight line fits were:

$$\sigma_u/u_* = 2.1 - 12 z/cu_* \quad \sigma_v/u_* = 1.7 - 8 z/cu_*$$

for near-neutral conditions. For the unstable Groups III, IV, and V both σ_u/u_* and σ_v/u_* increase slightly with height. The scatter is larger but straight line approximations would be valid for practical purposes. These are

$$\sigma_u/u_* = 2.3 + 6 z/cu_* \quad \sigma_v/u_* = 2.2 + 6 z/cu_*$$

for unstable conditions. The comments made on σ_w/u_* apply to these results as well.

5 Summary

The turbulence in the planetary boundary layer does seem amenable to scaling by fairly simple schemes. The best of the two sets proposed in the literature seems to be to scale the heights by h , the height to the inversion, velocities by $w_* = (ghQ/T)^{1/2}$ and temperatures by $\theta_* = (Q^2T/gh)^{1/2}$, for unstable stratifications. For neutral conditions u_* may be more appropriate for velocities. The experimental results were generally in agreement with the results of the numerical models developed by Deardorff (1972) and Wyngaard et al. (1974). It is evident, however, that further experimental studies are necessary to resolve the effects of surface roughness, baroclinicity, and the lack of time stationarity.

Acknowledgments

The data were collected during IFYGL and I am grateful to those who participated in its collection and analysis. J.I. MacPherson and N. Bobbit of NAE deserve special thanks. Thanks are also due to Dr B.R. Kerman for constructive discussions of the results.

References

- BROOKS, C.E.P. and N. CARRUTHERS. 1953. *Handbook of statistical methods in meteorology*. London: HMSO, 412 pp.
- CLARKE, R.H. and G.D. HESS. 1973. On the appropriate scaling for velocity and temperature in the planetary boundary layer. *J. Atmos. Sci.* **30**: 1346-53.
- DEARDORFF, J.W. 1972. Numerical inves-

- tigation of neutral and unstable planetary boundary layers. *J. Atmos. Sci.* **29**: 91-115.
- 1973. Three-dimensional numerical modeling of the planetary boundary layer. In *Workshop in micrometeorology*, ed. D.A. Haugen, pp. 271-311. Amer. Meteor. Soc.
- 1973. An explanation of anomalously large Reynolds stresses within the convective planetary boundary layer. *J. Atmos. Sci.* **30**: 1070-6.
- LENSCHOW, D.H. 1970. Airplane measurements of planetary boundary layer structure. *J. Appl. Meteor.* **9**: 874-84.
- MCBEAN, G.A. 1971. The variations of the statistics of wind, temperature and humidity fluctuations with stability. *Boundary-Layer Meteor.* **1**: 438-57.
- , and R.D. PATERSON. 1975. Variations of the turbulent fluxes of momentum, heat and moisture over Lake Ontario. *J. Phys. Oceano.* **5**: 523-31.
- , and J.I. MACPHERSON. 1976. Turbulence above Lake Ontario. *Boundary-Layer Meteor.* (accepted for publication).
- SMITH, S.D. 1973. *Thrust anemometer measurements over the sea re-examined*. Rep. BI-R-73-1, Bedford Institute of Oceanography, Dartmouth, Nova Scotia, Canada, 23 pp.
- TENNEKES, H. 1973. Similarity laws and scale relations in planetary boundary layers. In *Workshop in micrometeorology*, ed. D.A. Haugen, pp. 177-216. Amer. Meteor. Soc.
- WYNGAARD, J.C. 1973. On surface-layer turbulence. In *Workshop in micrometeorology*, pp. 101-49.
- ; O.R. COTE; and K.S. RAO. 1974. Modeling the atmospheric boundary layer. *Adv. in Geophys.* **18A**: 193-211.
-